

ELEMENTS OF LASER DEVICES

PACS numbers: 85.70.Sq; 42.60.By; 42.25.Lc
DOI: 10.1070/QE2013v043n08ABEH015122

Permanent-magnet Faraday isolator with the field intensity of 25 kOe

E.A. Mironov, I.L. Snetkov, A.V. Voitovich, O.V. Palashov

Abstract. **A Faraday isolator with a single magneto-optical element is constructed and experimentally tested. It provides the isolation ratio of 30 dB at an average laser radiation power of 650 W. These parameters are obtained by increasing the field intensity in the magnetic system of the isolator and employing a low-absorption magneto-optical element.**

Keywords: *Faraday isolator, isolation ratio, thermally induced birefringence, thermal lens.*

1. Introduction

As the average power of repetitively pulsed and cw lasers is steadily increasing, the problem of improvement of optical devices becomes more actual, and the key requirement is to suppress thermo-induced effects caused by absorption of radiation. One of such devices subjected to the heat self-action due to the relatively high ($\sim 10^{-3}$ cm^{-1}) absorption in magneto-optical elements (MOEs) is a Faraday isolator (FI) [1]. A nonuniform temperature distribution in the volume of the MOE leads to phase distortions (thermal lens), nonuniform distribution of the angle of the polarisation plane rotation caused by the temperature dependence of the Verdet constant, appearance of mechanical stresses and, hence, to the linear birefringence (photo-elastic effect) [2]. The isolation ratio for the FI is determined by the depolarisation of radiation due to the photo-elastic effect, whereas the contribution of the temperature dependence of the Verdet constant is negligible [2, 3]. Thus, at an increased radiation power the isolation ratio decreases. Hence, at a prescribed isolation ratio, the power of radiation passed through the FI cannot be higher than a limiting value $P_{\max}$. In commercial FIs, the characteristic power is $P_{\max} \approx 100$ W at the isolation ratio of 30 dB.

One approach to increase $P_{\max}$ is separation of a magneto-optical element into thin disks cooled through the optical surfaces [4]. Such a geometry results in a considerably lower temperature gradient and, hence, in lower temperature distortions in the disks. One more popular approach [2, 5–7] is based on the idea of thermo-depolarisation compensation. To this end, one MOE that rotates the polarisation plane by 45° is replaced by two MOEs with a reciprocal optical element between them. In this case, the distortions arising in passing through the first element are partially compensated while passing through the second one. Such FIs provide a reliable isolation ratio at a kilowatt power of the passing radiation [8, 9]. It is reasonable to employ a cryogenic FI [10, 11] and a FI with a superconducting solenoid used as a magnetic system (MS) [11] for the radiation of kilowatt (and higher) power. The methods for increasing $P_{\max}$ described above have drawbacks related to awkward complicated construction and expensive FIs. However, in our opinion, the possibilities of the traditional scheme with a single FI are not exhausted. A traditional isolator is described in [12] with the isolation ratio of 30 dB, which operates at a maximal radiation power of 400 W. The output power can be raised by increasing the field intensity in the MS of the isolator, and reducing the length of the employed MOE. It can be done by employing the magnetic materials with enhanced properties and improving the schematics of the MS. Achievements in the field of construction of magneto-active media give a chance to employ elements with lower absorption coefficients. All these factors result in a lower heat release in the MOE and, hence, lower thermo-induced depolarisation.

By depolarisation γ is meant the ratio

$$\gamma = \frac{P_1}{P_1 + P_2}, \tag{1}$$

where $P_{1,2}$ is the power of depolarised and main polarised radiation components, respectively. The isolation ratio I for an optical device, expressed in decibels is defined as

$$I = 10 \lg(1/\gamma). \tag{2}$$

Depolarisation γ arising due to the radiation absorption in optical elements of the FI and called 'hot' or 'thermally induced' depends on the power of optical radiation and length, geometry, and material constants of the MOE. For a cubic crystal with the [001] orientation

$$\gamma_{001} = A_0 p^2, \tag{3}$$

where

$$p = \frac{Q\alpha L P_{\mathrm{L}}}{\lambda\kappa}; \quad Q = \alpha_T \frac{n_0^3}{4} \frac{1+\nu}{1-\nu}(p_{11} - p_{12}); \tag{4}$$

λ and P_{L} are the radiation wavelength and power; L is the length of the MOE; α is the absorption index; κ is the thermal conductivity; p_{ij} are the photo-elastic coefficients; Q is the thermo-optical constant; α_T is the linear expansion factor; n_0 is the refraction index; and ν is the Poisson's ratio for the MOE material. For a Gaussian beam $A_0 = 0.014$. Such orien-

E.A. Mironov, I.L. Snetkov, A.V. Voitovich, O.V. Palashov Institute of Applied Physics, Russian Academy of Sciences, ul. Ul'yanova 46, 603950 Nizhnii Novgorod, Russia; e-mail: miea@rambler.ru

Received 23 January 2013
Kvantovaya Elektronika **43** (8) 740–743 (2013)
Translated by N.A. Raspopov

tation of a TGG crystal used in the FI gives a minimal thermo-induced depolarisation.

In the present work we describe the FI assembled in accordance with a conventional scheme which provides the isolation ratio of ~30 dB at a laser radiation power of up to ~650 W. Such a relatively high power P_{max} as compared to that reported in [12] is explained by the increased intensity of the magnetic field in the MS (by 20%) and employment of the MOE with a lower absorption coefficient. In Section 2 we describe the MS capable of achieving the magnetic field intensity of ~25 kOe in which, consequently, the length of the MOE may be shortened to only 9 mm.

2. Properties of the MS design

Obtaining high magnetic fields is a complicated technical problem. The residual induction of most strong modern permanent magnets does not exceed 14 kGs. The required magnetisation distribution in the MS that provides a maximal possible field intensity is similar to the dipole field distribution and can hardly be realised. A specific case is a MS with the magnets of only ring shapes having radial and axial directions of magnetisation. Such MSs are relatively simple in production; however, the axial-radial approximation has limitations in the field intensities (~20 kOe). Attempts to further increase the field by enlarging the MS dimensions lead to an unreasonably great mass of the magnet. This is related to a logarithmic dependence of the limiting achievable field at the MS axis on the ratio of external (D) to internal (d) diameters of the magnet:

$$H_z \sim \ln(D/d), \tag{5}$$

where z is the MS axis. A detailed analysis of the possibilities of such an axial-radial realisation is given in [12].

In addition, an attempt to employ ferromagnetic alloys with high residual induction in the previously used geometry did not result in the desired increase in the field intensity as compared to the maximal field in [12] that was ~21 kOe, because in this case the degaussing effect for a central part of the MS was enhanced. To solve this problem, the field over the entire volume of the MS was calculated including the domains occupied by the magnets. The domains were found most subjected to demagnetisation and it was suggested to remove the magnets from those places. A particular place and the quantity of the magnetic material to be removed were determined by using a specially developed software. As the result, the maximal field intensity in the MS calculated and realised in this way was increased to ~25 kOe, and the new method for preventing demagnetisation was tested. We plan to use the method in the future.

Presently, the most intensive fields are obtained in MSs with a considerably more complicated distribution of magnetisation. The method has many kinds and names: magic sphere, Halbach cylinder and so on [13–16]. However, it is very difficult to realise this idea. The complicated distribution of magnetisation is provided by the layers made of uniformly magnetised segments each having different thicknesses and particular directions of magnetisation at various radii.

In the considered MS we obtained the fields at the axis of above 25 kOe. The system is schematically shown in Fig. 1. It comprises four radial rings with the external diameter $D = 124$ mm and thickness $h = 28$ mm and a single axial ring at the centre with $D = 100$ mm, $h = 18$ mm and internal diameter

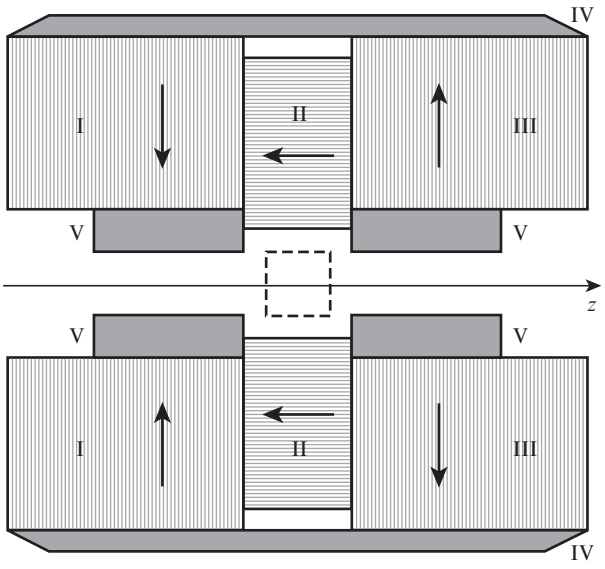

Figure 1. Schematic diagram of the magnetic system of the FI: domains I, III are radially magnetised rings; domain II is the axially magnetised ring; domains IV, V are a magnetic conductor; dashed rectangular is the TGG crystal.

$d = 21$ mm. The 'clear' aperture diameter of the MS was 13 mm. All the radial magnets have the residual induction $B_r = 1.32$ kGs, and for the radial ring it is 1.1 kGs. The MS has three magnetic conductors, one of them closes outside the poles of the radial magnets and serves as a case. More important are internal magnetic conductors. They are fabricated from pure iron with the saturation induction of 20.3 kGs.

The field distributions in the MS are shown in Fig. 2. The nonuniformity of the magnetic field integrated over the length of the TGG crystal (the relative difference of the angles of rotation of the polarisation plane at the aperture periphery and at its centre) is ~5% at $r = 6.5$ mm and ~2% at $r = 4$ mm. The total depolarisation of radiation in the isolator due to this nonuniformity was below 10^{-4}, which is by an order of magnitude lower than the thermo-induced depolarisation in the case of high-power operation.

The magnetic system was calculated by using two programs: the special program packet for the FI with large mag-

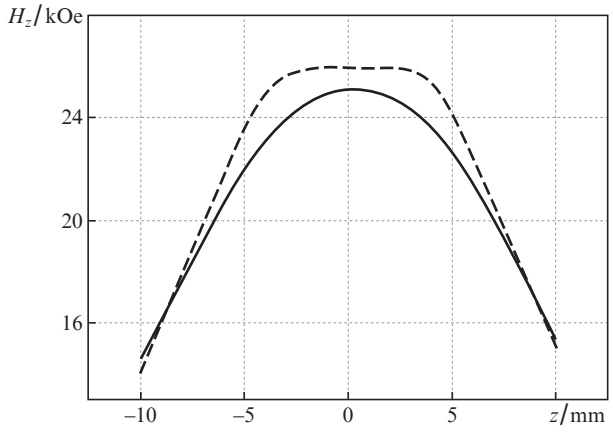

Figure 2. Calculated distribution of the magnetic field in the MS at $r = 0$ (solid curve) and 4 mm (dashed curve).

nets developed at the IAP RAS and the commercial product ELcut developed by the 'Tor' company (St. Petersburg).

3. Optical characteristics of the FI

The experimental setup is schematically shown in Fig. 3. Linearly polarised cw radiation at the wavelength of 1076 nm from a single-mode ytterbium fibre laser (*1*) (IPG Photonics) was simultaneously used as the heating and probe radiation. The MOE was a TGG crystal of length 9 mm and diameter 13 mm with the absorption coefficient $\alpha = 1.3\times10^{-3}$ cm^{-1}. The maximal laser power was 330 W. The laser radiation was directed to the FI (*2*) under study, then reflected from the mirror (*3*) with the reflection coefficient 99%, passed once again through the isolator and entered the absorber (*4*). Thus, the total power of the heating radiation passing though the MOE doubled. The heating of the MOE due to absorption resulted in depolarisation of the radiation. The weakened beam having passed the mirror was directed to the wedge (*5*) and divided into two orthogonally polarised beams. The depolarised component was directed to the CCD-camera (*6*). The rotation of the wedge (*5*) provided a control of the turning angle of the polarisation plane when the passing radiation power varied.

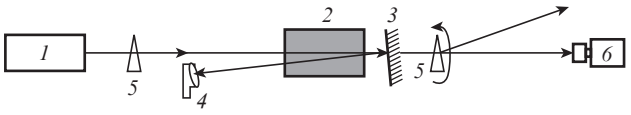

Figure 3. Experimental setup:
(*1*) ytterbium fibre laser; (*2*) FI under investigation; (*3*) mirror; (*4*) absorber; (*5*) wedges from Iceland spar; (*6*) CCD camera.

Note that γ may be completely determined both by thermal effects and by the 'cold' depolarisation, to which the quality of the MOE and the nonuniformity of the magnetic field may contribute. The dependence of depolarisation on the power of radiation passed through the FI is shown in Fig. 4. By a dashed line we designate the theoretical dependence (3) at k = 5 W m^{-1} K^{-1} [10], $Q = 17\times10^{-7}$ K^{-1} [10], and $\alpha = 1.3\times10^{-3}$ cm^{-1}.

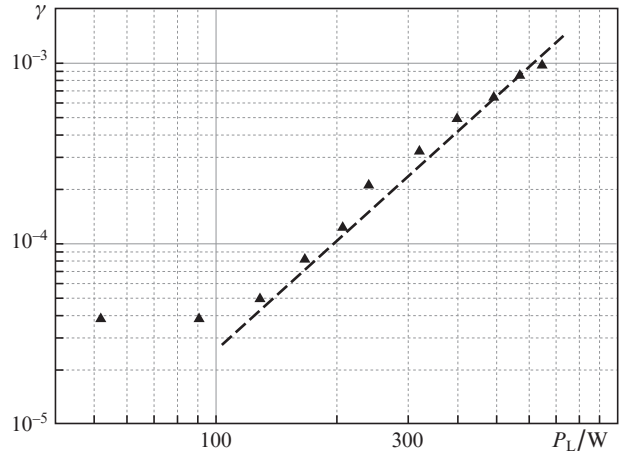

Figure 4. Depolarisation vs. the power of radiation passed through the FI under investigation. Dashed line corresponds to theoretical calculation (3).

One more significant characteristic of the FI is the angle of the polarisation plane rotation. When high-power radiation passes through the FI, the MOE is heated, which leads to a reduced angle of the polarisation plane rotation due to the temperature-dependent Verdet constant. If the angle of the polariser axis is adjusted, the influence of this effect on the isolation ratio can be neglected [3]. However, the inevitable consequence of the heating is a greater loss in the first transit of radiation through the FI. In Fig. 5 one can see that the increase in the radiation power from 0 to 400 W would reduce the angle of rotation by 1.4°, which corresponds to the losses of the radiation power in the FI ~0.06% in the first transit. Note, that this problem can be solved by stabilising the MOE temperature (for example, with a Peltier element [17]).

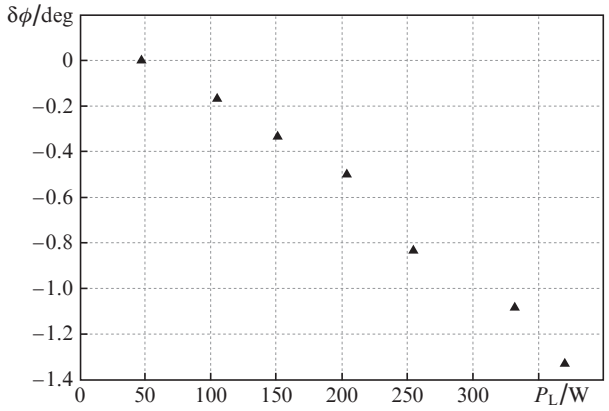

Figure 5. Variation of the angle of the polarisation plane rotation of radiation passing through the FI vs. the power.

One more important parameter of the FI is the warm-up period, because a certain time is required to heat the MOE to a constant temperature after the start. The experimentally measured dependence of the angle of the polarisation plane rotation for the radiation passed through the FI is shown in Fig. 6 as a function of the duration of operation. One can see that it requires ~5 min for the FI to reach a steady state at the radiation power of 650 W.

The focal length F of the thermal lens arising in the MOE was measured. The results are presented in Fig. 7 and well

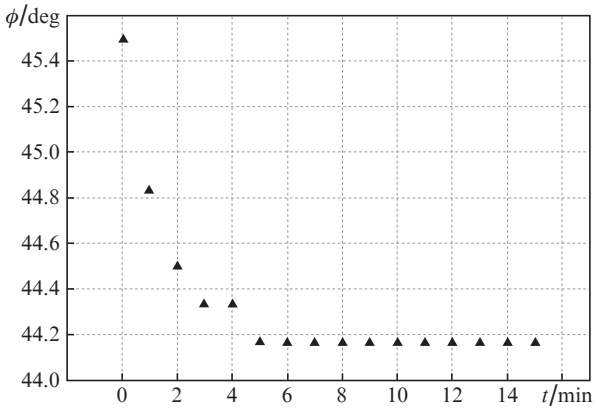

Figure 6. Angle of the polarisation plane rotation of 650-W radiation passing through the FI vs. time of its operation.

agree with the theoretical results calculated by the formula from [18]:

$$F = \frac{4\pi\kappa a^2}{P_L L \alpha Q},$$

where $Q = 17\times10^{-7}$ K^{-1}; a is the radius of a Gaussian beam at the 1/e level, which in the present experiment is 0.97 mm. At the radiation power of 650 W the focal length of the thermal lens was 4 m.

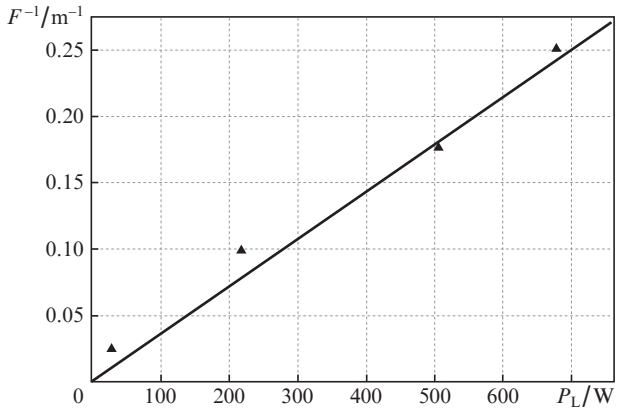

Figure 7. Inverse focal distance of the thermal lens vs. the power of heating radiation. Points are the experiment and solid line is the calculation.

It is important that the reduction in the MOE length due to the increased magnetic field intensity not only reduces the heat release, but, approaching the element geometry to the disk geometry, also opens new possibilities for ensuring heat removal through optical surfaces of the MOE [19, 20]. If a front heat removal is provided in the FI under study, for example, by the optical welding of the MOE and YAG crystals suggested in [21] then with the actual aspect ratio D/L of the magneto-optical element, the thermally induced depolarisation can be additionally lowered by ~20%. A replacement of the MOE from TGG crystal by TAG ceramics [22, 23] in the FI under consideration may reduce γ by a factor of 1.8. In this case, γ will reduce by a factor of 1.3 due to the MOE length shortening because of the greater (by ~30% [22,23]) TAG-ceramics Verdet constant and by a factor of 1.4 due to a more efficient employment of the disk geometry [19, 20]. Such improvement of the MOE of the Faraday isolator with a retained MS may increase the admissible radiation power up to 1 kW at the same isolation ratio of 30 dB.

4. Conclusions

In the present work the FI designed in accordance with the conventional scheme was experimentally investigated and exhibited the isolation ratio of ~30 dB at the average laser radiation power of ~650 W. Such a high operating power is explained by the two factors. First, the field intensity in the MS was successfully increased to 25 kOe, which made it possible to shorten the MOE length. Second, for the MOE we employed a TGG crystal with a lower absorption coefficient. These two factors lowered the heat release in the MOE caused by absorption of laser radiation in it and thereby reduced the thermo-induced depolarisation.

In fabricating the MS of the optical isolator, the method for preventing demagnetisation of its central part was tested. Further improvement and employment of this method will help realising even more intensive fields and, hence, employment of shorter MOEs.

References

1. Zarubina T.V., Petrovskii G.T. *Opt. Zh*., **59**, 48 (1992).
2. Khazanov E.A. *Kvantovaya Elektron*., **26**, 59 (1999) [*Quantum Electron*., **29**, 59 (1999)].
3. Khazanov E.A., Kulagin O.V., Yoshida S., Tanner D., Reitze D. *IEEE J. Quantum Electron.*, **35**, 1116 (1999).
4. Mukhin I.B., Khazanov E.A. *Kvantovaya Elektron.*, **34**, 973 (2004) [*Quantum Electron*., **34**, 973 (2004)].
5. Khazanov E.A. *Kvantovaya Elektron*., **31**, 351 (2001) [*Quantum Electron*., **31**, 351 (2001)].
6. Khazanov E., Andreev N., Palashov O., Poteomkin A., Sergeev A., Mehl O., Reitze D. *Appl. Opt.*, **41** (3), 483 (2002).
7. Andreev N.F., Palashov O.V., Potemkin A.K., Reitze D.H., Sergeev A.M., Khazanov E.A. *Kvantovaya Elektron*., **30**, 1107 (2000) [*Quantum Electron*., **30**, 1107 (2000)].
8. Voitovich A.V., Katin E.V., Mukhin I.B., Palashov O.V., Khazanov E.A. *Kvantovaya Elektron*., **37**, 471 (2007) [*Quantum Electron*., **37**, 471 (2007)].
9. Nicklaus K., Daniels M., Hohn R., Hoffmann D., in *Advanced Solid-State Photonics* (Incline Village, Nevada, USA, 2006) p. MB7.
10. Zheleznov D.S., Khazanov E.A., Mukhin I.B., Palashov O.V. *Proc. 12th Conf. on Laser Optics* (St. Petersburg, 2006) TuR1–p21.
11. Zheleznov D.S., Khazanov E.A., Mukhin I.B., Palashov O.V., Voytovich A.V. *IEEE J. Quantum Electron.*, **43**, 451 (2007).
12. Mukhin I.B., Voitovich A.V., Palashov O.V., Khazanov E.A. *Opt. Commun.*, **282**, 1969 (2009).
13. Trenec G., Volondat W., Cugat O., Vigue J. *Appl. Opt.*, **50** (24), 4788 (2011).
14. Zijlstra H. *Philips J. Res*., **40**, 259 (1985).
15. Halbach K. *Nucl. Instrum. Methods*, **169**, 1 (1980).
16. Halbach K. *Nucl. Instrum. Methods*, **187**, 109 (1981).
17. Palashov O.V., Ievlev I.V., Perevezentsev E.A., Katin E.V., Khazanov E.A. *Kvantovaya Elektron.*, **41**, 858 (2011) [*Quantum Electron*., **41**, 858 (2011)].
18. Perevezentsev E., Poteomkin A., Khazanov E.A. *Appl. Opt.*, **46** (5), 774 (2007).
19. Zheleznov D.S., Khazanov E.A., Mukhin I.B., Palashov O.V. *Proc. SPIE Int. Soc. Opt. Eng.*, **6610**, 66100F (2007).
20. Zheleznov D.S., Starobor A.V., Palashov O.V., Khazanov E.A. *J. Opt. Soc. Am. B*, **29**, 4 (2012).
21. Mukhin I.B., Perevezentsev E.A., Palashov O.V. *Proc. 15th Conf. on Laser Optics* (St. Petersburg, 2012) ThR1–p27.
22. Lin H., Zhou S., Teng H. *Opt. Mater.*, **33**, 1833 (2011).
23. Geho M., Sekijima T., Fujii T. *J. Cryst. Growth*, **267**, 188 (2004).